Defense and tolerance technique against attacks and faults on leader-following multi-USVs

Chun Liu, *Member, IEEE,* Zhiwei Xia, Yongxiao Tian, *Member, IEEE,* and Ron J. Patton, *Life Fellow, IEEE*

***Abstract*—This study explores the leader-following consensus tracking control issue of multiple unmanned surface vehicles (multi-USVs) in the presence of malicious connectivity-mixed attacks in the cyber layer, and concurrent output channel noises, sensor/actuator faults, and wave-induced disturbances in the physical layer. Sensor/actuator faults are initially modeled with unified incipient and abrupt features. Additionally, connectivity-mixed attacks are depicted using connectivity-paralyzed and connectivity-maintained topologies through nonoverlapping and switching iterations. The standardization and observer design in multi-USVs are incorporated to decouple the augmented dynamics and estimate unknown state, fault, and noise observations, and then a defense and fault-tolerant consensus tracking control approach is designed to accomplish the robustness to disturbances/noises, resilience to attacks, and tolerance to faults, simultaneously. The criteria for achieving leader-following exponential consensus tracking of multi-USVs with cyber-physical threats can be determined based on activation rate and attack frequency indicators. Comparative simulations outline the effectiveness and economy of the proposed defense and tolerance technique against sensor/actuator faults and cyber-attacks on multi-USVs.**

***Index Terms*—Defense and tolerance technique, fault-tolerant consensus tracking, multi-USVs, actuator and sensor faults, cyber-attacks**

I. Introduction

WITH increasing worldwide interest in scientific, commercial, and military issues in shallow waters and oceans, there is a powerful demand for the advancement of intelligent USVs with more autonomous, reliable, and advanced capabilities to greatly expand the diversity and breadth of USV missions [1]. Recent progress of guidance and control methodologies for marine vehicles is comprehensively overviewed in [2]. Diverse literature on cooperation and coordination of multi-USVs includes, but is not limited to, consensus control [3], flocking control [4], path following [5], and formation control [6]. The networked multi-USVs, as typical cyber-physical multi-agent systems, are susceptible to physical constraints, including completely unknown model parameters and environmental disturbances induced by winds, waves, and currents, as well as to the networked constraints, including network-induced delays and packet loss and connectivity maintenance of communication topologies.

Compared to various existing attacks, i.e., state-dependent attacks [7], actuator attacks [8], denial-of-service (DoS) attacks [9], [10], deception attacks [11] and even hybrid attacks [12], [13], advanced USVs that configure computing and digital systems become more vulnerable and susceptible to a disruption of information transmission due to cyber-attacks and communication hardware or software flaws. Secure consensus tracking control, especially for networked leader-following multi-USVs requires continuous, non-disruptive, and precise information interaction between individual USVs, which inherently conflicts with the devastation of ideal communication topologies under cyber-attacks. Existing well-established techniques [7], [11] for undirected or directed balanced topologies are unable to effectively and intuitively solve the leader-following tracking problem of multi-USVs under attacks with defense features. Therefore, a novel defense technique-based leader-following consensus tracking development for multi-USVs, in response to connectivity-mixed cyber-attacks causing specific topology switching (connectivity-maintained and connectivity-paralyzed properties), is informative but challenging. The maneuvering and manipulation of networked USVs are influenced not only by crippled topologies caused by attacks but also by physical actuator faults [14], [15] or sensor faults [16]. In contrast to fault detection and accommodation approaches [17], [18] that focus on detecting, locating, and isolating faults, fault estimation [19], [20] and fault-tolerant control schemes [21], [22], [23], [24] have attracted substantial attention to improving the safety, reliability and excellent tracking performance of multi-USVs. The tolerance technique-based robust nonlinear control protocol is developed for multiple cyber-physical USVs with probabilistic actuator faults and time-varying communication delays by utilizing Lyapunov-Krosovskii functional [25]. Fault-tolerant frameworks associated with adaptive fuzzy backstepping [26] and event-triggered adaptive neural networks [27] are proposed to address unknown dynamics, external disturbances, and actuator saturation. In addition, a unified fault model (e.g., stuck, hard-over, bias, partial, and total faults) is established in USV dynamics and the quantized sliding mode tolerant technique is then proposed to suppress the negative impact of physical offsets [28]. Typically lower-cost USVs cannot be equipped with all sensing devices (e.g., radar, laser, vision, ultrasound, sonar, compass, or GPS) that can measure internal state information, and the tracking control based on full state information [11] is more difficult to realistically achieve.

This work was supported by National Natural Science Foundation of China (62103250, 62273223, 62333011, and 62336005); Project of Science and Technology Commission of Shanghai Municipality, China (22JC1401401); Shanghai Sailing Program (21YF1414000).

C. Liu is with the School of Mechatronic Engineering and Automation, and also with the Institute of Artificial Intelligence, Shanghai University, Shanghai 200444, China (e-mail: Chun_Liu@shu.edu.cn).

Z. W. Xia is with the School of Mechatronic Engineering and Automation, Shanghai University, Shanghai 200444, China (e-mail: xzw_shu@shu.edu.cn)

Y. X. Tian is with the School of Future Technology, Shanghai University, Shanghai 200444, China (e-mail: yx_tian@shu.edu.cn)

R. J. Patton is with the School of Engineering and Computer Science, University of Hull, Hull HU6 7RX, U.K. (e-mail: r.j.patton@hull.ac.uk).

Considering the unavailable state information (sway, yaw, and roll velocities), a secure consensus tracking strategy should be integrated with output angular data, thus greatly enabling local tolerance and global tracking of multiple USVs while encountering simultaneous sensor/actuator faults, channel noises, and wave-induced disturbances.

However, quite limited literature has been conducted on defense and tolerance techniques in simultaneously compensating physical faults and resisting attacks in multi-USVs for a safe and healthy response to cyber-physical threats, with the following emphasis. The resilient event-triggered fault detection issue is solved for USVs under DoS jamming attacks, external disturbances, and system faults [29] and the exponential stability with a weighted H_∞ performance is guaranteed. A co-designed framework of observer-based fault detection filter and the event-based controller is constructed to mitigate the adverse effect of hostile aperiodic DoS attacks, communication delays, and actuator faults [30]. To broaden the perspective to fault-tolerance and anti-attack defense strategies for multiagent systems (MASs) [31], several studies are already emerging. For example, anomaly detection and identification of MASs with false-data-injection attacks and physical faults [32], cooperative tracking of nonlinear MASs subject to composite faults under connectivity-mixed attacks [13], [33], and resilient consensus control issues for heterogeneous linear MASs [34], uncertain Takagi–Sugeno nonlinear MASs [35], heterogeneous nonlinear second-order MASs [36] even with DoS attacks and actuator faults.

The main findings of this study can be outlined as follows. (i) In comparison to the consensus tracking of multi-USVs in resisting independent cyber-attacks [7], [11], or compensating individual faults [15], [16], it is an endeavor to combine the unified fault modeling, attack defense, and fault tolerance technologies effectively. It can synergistically address composite constraints in both the physical and cyber layers, handling unified faults, disturbances, and noises in the physical layer while coping with maintained/paralyzed topological connectedness in the cyber layer. (ii) Unlike the separated estimation and tolerance procedure that disregards the direct utilization of estimated information from observation to control layers, standardization and estimation-based observer techniques are utilized to detach the design of the expanded multi-USVs and mitigate the adverse impacts arising from unexplored states, faults, and noisy records. Additionally, to achieve a balance between the effectiveness of attack metrics and economy in terms of fault tolerance, attack resilience, and disturbance/noise robustness, the average dwelling time (ADT) index [33] is replaced by dual-constraint indicators, namely attack frequency and activation rate. This substitution intuitively establishes an online update connection between the leader-following exponential cooperative tracking achievement and the more progressive dual assault indicators.

The remaining portion of this study is laid out as follows. Section II introduces the problem formulation. Section III develops the standardization/observer and defense/tolerance protocols. Simulations in Section IV illustrate the efficacy and advantage of the defense and tolerance technique on multi-USVs. Ultimately, Section V delivers conclusions.

II. Problem Formulation

A. Graph theory

A directed and switching graph $\mathcal{G}_{\gamma(t)}$ is defined as a pair $(\nu, \varepsilon, \mathcal{A}_{\gamma(t)})$ associated with a switching signal $\gamma(t)$. Here, $\nu = \{\nu_1, \nu_2, \cdots, \nu_N\}$ represents a nonempty finite set of nodes, $\varepsilon \subseteq \nu \times \nu$ denotes a set of edges, and (ν_i, ν_j) indicates an edge between the ordered node pair ν_i, ν_j. The adjacency matrix of $\mathcal{G}_{\gamma(t)}$, represented as $\mathcal{A}_{\gamma(t)} = [a_{ij}^{\gamma(t)}] \in \mathbb{R}^{N\times N}$, signifies the weight coefficient of (ν_i, ν_j) as $a_{ij}^{\gamma(t)}$, where $a_{ii}^{\gamma(t)} = 0$ and $a_{ij}^{\gamma(t)} > 0$ if $(\nu_i, \nu_j) \in \varepsilon$, and $a_{ij}^{\gamma(t)} = 0$ otherwise. The Laplacian matrix, denoted as $\mathcal{L}_{\gamma(t)} = \mathcal{D}_{\gamma(t)} - \mathcal{A}_{\gamma(t)} = [l_{ij}^{\gamma(t)}] \in \mathbb{R}^{N\times N}$, incorporates a diagonal matrix $\mathcal{D}_{\gamma(t)} = [d_{ii}^{\gamma(t)}] \in \mathbb{R}^{N\times N}$ with $d_{ii}^{\gamma(t)} = \sum_{j=1}^{N} a_{ij}^{\gamma(t)}$.

The leader-following connection matrix, denoted as $\mathcal{H}_{\gamma(t)}$, is defined as the sum of the Laplacian matrix $\mathcal{L}_{\gamma(t)}$ and the information connection matrix $\mathcal{B}_{\gamma(t)}$. The information connection matrix $\mathcal{B}_{\gamma(t)}$ is represented as $\mathrm{diag}\{b_1^{\gamma(t)}, \cdots, b_N^{\gamma(t)}\}$, where $b_i^{\gamma(t)}$ represents the connection status between node ν_i and the leader. When $b_i^{\gamma(t)} = 1$, it indicates that node ν_i can access the leader through a directed path. On the other hand, if $b_i^{\gamma(t)} = 0$, it means that node ν_i has no direct connection to the leader.

B. USVs with actuator/sensor fault modeling

The asymmetric USV motions in the sway, yaw, and roll channels are considered, and the surge, heave, and pitch motions of the USV modeling are regarded as channel disturbances. In the leader-following multi-USVs, the sway, yaw, and roll motions of the ith following USV in the presence of rudder angle faults (actuator fault type) and wave-induced disturbances when the partial hydrodynamic effect is neglected are established as follows [17]:

$$\begin{cases} \dot{v}_i &= -\frac{1}{T_v} v_i + \frac{K_{dv}}{T_v}\left(\delta_i + f_{\delta i}^{v}\right) \\ \dot{r}_i &= \frac{K_{vr}}{T_r} v_i - \frac{1}{T_r} r_i + \frac{K_{dr}}{T_r}\left(\delta_i + f_{\delta i}^{r}\right) + \frac{1}{T_r}\omega_{\psi i} \\ \dot{\psi}_i &= r_i \\ \dot{p}_i &= \omega_n^2 K_{vp} v_i - 2\zeta\omega_n p_i - \omega_n^2 \phi_i + \omega_n^2 \omega_{\phi i} \\ & \quad + \omega_n^2 K_{dp}\left(\delta_i + f_{\delta i}^{p}\right) \\ \dot{\phi}_i &= p_i \end{cases} \tag{1}$$

where v_i, r_i, ψ_i, p_i and ϕ_i denote the sway velocity, yaw velocity, yaw angle, roll velocity, and roll angle, respectively, δ_i denotes the rudder angle (input only), $\omega_{\psi i}$ and $\omega_{\phi i}$ denote the wave-induced disturbances, $f_{\delta i}^{v}, f_{\delta i}^{r}$ and $f_{\delta i}^{p}$ denote the rudder angle actuator faults in the input channel, ω_n and ζ denote the natural frequency without damping and damping ratio, T_v and T_r denote the time constants, and $K_{dv}, K_{dr}, K_{vr}, K_{dp}$ and K_{vp} denote the channel gains.

The dynamics of the following USV with actuator/sensor faults, wave-induced disturbances, and output channel noises in the physical layer are characterized as

$$\begin{cases} \dot{x}_i(t) &= Ax_i(t) + B\delta_i(t) + F_a f_{ai}(t) + E_1\omega_{i1}(t) \\ y_i(t) &= Cx_i(t) + F_s f_{si}(t) + E_2\omega_{i2}(t) \end{cases} \tag{2}$$

where $x_i(t) = [v_i \;\; r_i \;\; \psi_i \;\; p_i \;\; \phi_i]^T, y_i = [\psi_i \;\; \phi_i]^T$ and $\omega_{i1}(t) = [\omega_{\psi i} \;\; \omega_{\phi i}]^T$ denote the intrinsic state, obtainable

output by angular sensors and external wave-induced disturbance, respectively, $f_{ai}(t) = [f_{\delta i}^{v} \ f_{\delta i}^{r} \ f_{\delta i}^{p}]^T$ denotes the actuator fault, and $f_{si}(t) \in \mathbb{R}^2$ and $\omega_{i2} \in \mathbb{R}^2$ denote the sensor fault and measuring output channel noise. $A, B = [\frac{K_{dv}}{T_v} \ \frac{K_{dr}}{T_r} \ 0 \ \omega_n^2 K_{dp} \ 0]^T, C$ stand for the system-identified matrices with C^T given as full column rank, E_1, E_2 denote the disturbance and noise-described gains, and F_a, F_s signify the fault-identified matrices. Specifically, A, F_a and E_1 are expressed as

$$A = \begin{bmatrix} -\frac{1}{T_v} & 0 & 0 & 0 & 0 \\ \frac{K_{vr}}{T_r} & -\frac{1}{T_r} & 0 & 0 & 0 \\ 0 & 1 & 0 & 0 & 0 \\ \omega_n^2 K_{vp} & 0 & 0 & -2\varsigma\omega_n & -\omega_n^2 \\ 0 & 0 & 0 & 1 & 0 \end{bmatrix}$$
$$F_a = \begin{bmatrix} \frac{K_{dv}}{T_v} & 0 & 0 \\ 0 & \frac{K_{dr}}{T_r} & 0 \\ 0 & 0 & 0 \\ 0 & 0 & \omega_n^2 K_{dp} \\ 0 & 0 & 0 \end{bmatrix}, E_1 = \begin{bmatrix} 0 & 0 \\ \frac{1}{T_r} & 0 \\ 0 & 0 \\ 0 & \omega_n^2 \\ 0 & 0 \end{bmatrix} \quad (3)$$

Sensor and actuator faults: $f_{ai}(t) = [f_{\delta i}^{v} \ f_{\delta i}^{r} \ f_{\delta i}^{p}]^T$ and $f_{si}(t) = [f_{si}^{1}(t) \ f_{si}^{2}(t)]^T$ denote the unified time-dependent faults in actuators and sensors, including abrupt and incipient types in the input and output channels, and each element is modeled as

$$\begin{cases} f_{\delta i}^{\varrho}(t) & = \left(1 - e^{-\epsilon_a^{\varrho}(t - T_a^{\varrho})}\right) \bar{f}_{\delta i}^{\varrho}, t \geq T_a^{\varrho}, \varrho = v, r, p \\ f_{si}^{\varrho}(t) & = \left(1 - e^{-\epsilon_s^{\varrho}(t - T_s^{\varrho})}\right) \bar{f}_{si}^{\varrho}, t \geq T_s^{\varrho}, \varrho = 1, 2 \end{cases} \quad (4)$$

where $\bar{f}_{\delta i}^{\varrho}$ and $\bar{f}_{si}^{\varrho}$ are the elements in the ϱth row with undetermined constant fault limits, T_a^{ϱ} and T_s^{ϱ} are fault occurrence time instants, and ϵ_a^{ϱ} and ϵ_s^{ϱ} denote the unidentified decay rates. The individual sensor and actuator faults can be classified as incipient-type faults (characterized by a gradually varying decay rate) when $\underline{\epsilon}_{a(s)} \leq \epsilon_{a(s)} < \bar{\epsilon}_{a(s)}$. On the other hand, they are considered abrupt-type faults (characterized by a rapidly varying decay rate) when $\epsilon_{a(s)} \geq \bar{\epsilon}_{a(s)}$.

The dynamics of the leading USV (designated as 0) without actuator/sensor faults, wave-induced disturbances, and output channel noises are identified as

$$\dot{x}_0(t) = Ax_0(t) + B\delta_0(t), y_0(t) = Cx_0(t) \quad (5)$$

where the state vector $x_0(t) = [v_0 \ r_0 \ \psi_0 \ p_0 \ \phi_0]^T$ and output vector $y_0 = [\psi_0 \ \phi_0]^T$ of the leading USV can be measured by angle/angular velocity sensors. Hence, the control input, i.e., the rudder angle is formulated as $\delta_0(t) = -K_x x_0(t)$ with the later derived estimation matrix $K_x \in \mathbb{R}^{1\times 5}$.

Assumption 1: The incipient and abrupt sensor and actuator faults in a unified manner exhibit differentiable characteristics after specific instances of fault occurrence. The decay rates of these faults, denoted as ϵ_a^{ϱ} and ϵ_s^{ϱ}, are manually determined with the aid of known constants $\bar{\epsilon}_{a(s)} > 0$ and $\underline{\epsilon}_{a(s)} > 0$, which represent the upper and lower bounds, respectively.

Assumption 2: (i) The wave-induced disturbances on the yaw velocity and roll velocity channels are limited by positive and known upper bounds, i.e., $|\omega_{\psi i}(t)| \leq \bar{\psi}_i$ and $|\omega_{\phi i}(t)| \leq \bar{\phi}_i$. (ii) The first-/second-order derivatives of the measuring noise in the output channel are bounded in form of $\|\omega_{i2}(t)\| \leq \bar{\omega}_i$ and $\|\dot{\omega}_{i2}(t)\| \leq \bar{\mathcal{W}}_i$, respectively.

C. Connectivity-mixed attack modeling

To represent every topology transition caused by malicious attacks, a signal $\gamma(t) : [0, \infty) \to \Gamma = \{1, \cdots, r\}$ is brought in. The set $\{\mathcal{G}_1, \cdots, \mathcal{G}_r\}$ signifies the switching topologies $\mathcal{G}_{\gamma(t)}$, while $\{\mathcal{H}_1, \cdots, \mathcal{H}_r\}$ signifies the leader-following interaction matrices $\mathcal{H}_{\gamma(t)}$ associated with $\gamma(t) \in \Gamma$.

Connectivity-mixed attacks: The different topologies exhibit distinct outcomes: one preserves cyber connectivity while the other induces paralysis. Firstly, the connectivity-maintained topology, achieved by slightly altering or reconfiguring edges, retains its connectedness and includes a directed spanning tree with the leader serving as the root. Conversely, the connectivity-paralyzed topology, resulting from significant changes in edge connections, becomes disconnected and lacks a directed spanning tree. However, this state can be reversed through the utilization of attack defense and repair mechanisms to restore connectivity. The signal $\gamma(t) \in \Gamma = \Gamma_m \cup \Gamma_p = \{1, \cdots, q, q+1, \cdots, r\}, r \geq 2$ is introduced for switching topologies $\{\mathcal{G}_1, \cdots, \mathcal{G}_q, \mathcal{G}_{q+1}, \cdots, \mathcal{G}_r\}$, where Γ_m and Γ_p denote the q connectivity-maintained topology set and $(r-q)$ connectivity-paralyzed topology set, respectively.

Definition 1 [33]: Define the switching sequence as $k \in \mathbb{N}$ and the number of connectivity-mixed attacks as $N_\Gamma(t_0, t) = N_{\Gamma_m}(t_0, t) + N_{\Gamma_p}(t_0, t), \forall t > t_0 \geq 0$ with the numbers of connectivity-maintained/-paralyzed topologies $N_{\Gamma_m}(t_0, t)$ and $N_{\Gamma_p}(t_0, t)$, respectively. Denote $\mathcal{F}_\Gamma(t_0, t) = \frac{N_\Gamma(t_0, t)}{t - t_0}$ as the attack frequency over $[t_0, t)$.

Definition 2 [33]: Denote $\mathcal{R}_{\Gamma_m}(t_0, t) = \frac{T_m(t_0, t)}{t - t_0}$ and $\mathcal{R}_{\Gamma_p}(t_0, t) = \frac{T_p(t_0, t)}{t - t_0}$ as the connectivity-maintained and connectivity-paralyzed activation rates over $[t_0, t)$ for $\gamma(t) \in \Gamma_m$ and $\gamma(t) \in \Gamma_p$, where the total duration of activation for the connectivity-maintained and connectivity-paralyzed topologies, denoted as $T_m(t_0, t)$ and $T_p(t_0, t)$ respectively, can be represented as follows

$$\begin{cases} T_m(t_0, t) & = \sum_{k \in \mathbb{N}, \gamma(t_k) \in \Gamma_m} (t_{k+1} - t_k) \\ T_p(t_0, t) & = \sum_{k \in \mathbb{N}, \gamma(t_k) \in \Gamma_p} (t_{k+1} - t_k) \end{cases} \quad (6)$$

Definition 3: The control objective is centered around developing defense and tolerance techniques for the modeled multi-USVs (2) to effectively address various challenges including connectivity-mixed attacks, as well as actuator/sensor faults, wave-induced disturbances, output noises in the cyber-physical layer. Specifically, the leader-following consensus tracking issue of multi-USVs is addressed for $\forall t \geq t_0$ if there exists the decay rate $\lambda > 0$ and magnitude $\mu > 0$ such that

$$\|x_i(t) - x_0(t)\|^2 \leq \mu e^{-\lambda(t - t_0)} \|x_i(t_0) - x_0(t_0)\|^2 \quad (7)$$

Lemma 1 [37]: The matrix $\Upsilon_{\gamma(t)} = \Phi_{\gamma(t)} \mathcal{H}_{\gamma(t)} + \mathcal{H}_{\gamma(t)}^T \Phi_{\gamma(t)}$ possesses the following characteristics: it is symmetric and positive-definite. Here, $\Phi_{\gamma(t)} = \text{diag}\{\phi_{\gamma(t),1}^{-1}, \cdots, \phi_{\gamma(t),N}^{-1}\}$ is a diagonal positive-definite matrix. The elements $\phi_{\gamma(t),i}$, with i ranging from 1 to N, correspond to the entries of the vector $\phi_{\gamma(t)} = (\mathcal{H}_{\gamma(t)}^{-1})^T 1_N$. Additionally, $1_N = [1, \cdots, 1]^T \in \mathbb{R}^N$ represents a vector with all elements equal to 1. These properties hold for all $\gamma(t)$ within the set Γ.

Remark 1: (i) The USV dynamics (A, B) and (A, C) are controllable and detectable, respectively. (ii) Compared to

individual gain constraint and actuator faults [14], actuator faults and unmodeled dynamics [15], and multiple fault modes involving sensors and propellers [16], abrupt and incipient actuator/sensor faults in input and output channels are presented based on low-complexity descriptions compared to existing conventional fault modeling literature and are modeled with general exponential forms in Assumption 1, without the aid of any adaptive or auxiliary classification mechanisms. This builds a unified bridge between abrupt and incipient faults of multi-USVs. (ii) The physical implications of the initial and incipient failure of USV motions involve leaks, small changes in rudder angle caused by the aging of the physical structure, as well as wave, swell, or surge flows that can result in low amplitude failures and sudden jumps in rudder angle. (iii) In comparison to the measurement noise and packet loss that occur during measurement transmission [20], our analysis also takes into account wave-induced disturbances in the input channel and noise in the output channel. To accommodate these factors, a more comprehensive norm-bounded canonical constraint is utilized in Assumption 2.

Remark 2: In complex, open, and dynamic marine environments, there is a weak connectivity condition between shore-based stations and off-shore USVs, as well as between leading and following USVs. This vulnerability makes the connectivity topology of multi-USVs susceptible to switching or disruption by hybrid connectivity attacks, resulting in two outcomes: maintaining the connectivity topology or paralyzing it. In contrast to studies on heterogeneous hydrodynamics under actuator attacks [8] and communication constraints and DoS attacks [10], our model incorporates topologies based on a switched signal to represent the maintained and paralyzed connectedness. These topologies correspond to two cases: one with directed spanning trees and the other without spanning trees. Furthermore, even though a malicious attacker may use different attack nodes, moments of action, and durations, and the sensing capabilities of the unmanned defense equipment may face limitations in accurately ascertaining the real-time situation, it is still feasible and explicit to obtain the topology or sequence of switching during the response task interval by primarily relying on communication re-linking between the vehicles. The repair mechanism approach utilizes a model-based observer to monitor system behavior, triggering an attack alert when deviations exceed a threshold. Other strategies, i.e., adaptive scheme and dynamic topology adjustment mechanisms, can enhance system robustness, ensuring stable operation and secure communication in the face of attacks.

III. Main Results

A. Standardization and observer design

The process of normalizing the multi-USVs is defined using the augmented uncertainty and state components from (2), as shown below.

$$\dot{\bar{x}}_i(t) = \bar{A}\bar{x}_i(t) + \bar{B}\delta_i(t) + \bar{D}\bar{d}_i(t), y_i(t) = \bar{C}\bar{x}_i(t) \tag{8}$$

where $\bar{x}_i(t) = [x_i^T(t)\ f_{ai}^T(t)\ f_{si}^T(t)\ \omega_{i2}^T(t)]^T$, $\bar{d}_i(t) = [\omega_{i1}^T(t)\ \dot{f}_{ai}^T(t)\ \dot{f}_{si}^T(t)\ \dot{\omega}_{i2}^T(t)]^T$, and $\bar{A}, \bar{B}, \bar{C}$ and $\bar{D}$ are represented as

$$\bar{A} = \begin{bmatrix} A & F_a & \mathbf{0}_{5\times2} & \mathbf{0}_{5\times2} \\ \mathbf{0}_{3\times5} & \mathbf{0}_{3\times3} & \mathbf{0}_{3\times2} & \mathbf{0}_{3\times2} \\ \mathbf{0}_{2\times5} & \mathbf{0}_{2\times3} & \mathbf{0}_{2\times2} & \mathbf{0}_{2\times2} \\ \mathbf{0}_{2\times5} & \mathbf{0}_{2\times3} & \mathbf{0}_{2\times2} & \mathbf{0}_{2\times2} \end{bmatrix}, \bar{B} = \begin{bmatrix} B \\ \mathbf{0}_{3\times1} \\ \mathbf{0}_{2\times1} \\ \mathbf{0}_{2\times1} \end{bmatrix}$$
$$\bar{D} = \begin{bmatrix} E_1 & \mathbf{0}_{5\times3} & \mathbf{0}_{5\times2} & \mathbf{0}_{5\times2} \\ \mathbf{0}_{3\times2} & I_3 & \mathbf{0}_{3\times2} & \mathbf{0}_{3\times2} \\ \mathbf{0}_{2\times2} & \mathbf{0}_{2\times3} & I_2 & \mathbf{0}_{2\times2} \\ \mathbf{0}_{2\times2} & \mathbf{0}_{2\times3} & \mathbf{0}_{2\times2} & I_2 \end{bmatrix}, \bar{C} = \begin{bmatrix} C^T \\ \mathbf{0}_{3\times2} \\ F_s^T \\ E_2^T \end{bmatrix}^T \tag{9}$$

Define $\hat{\bar{x}}_i(t) = z_i(t) + Hy_i(t)$ with $\hat{\bar{x}}_i(t) = [\hat{x}_i^T(t)\ \hat{f}_{ai}^T(t)\ \hat{f}_{si}^T(t)\ \hat{\omega}_{i2}^T(t)]^T$ denoted by the estimation of $\bar{x}_i(t)$, where $\hat{f}_{si}(t), \hat{f}_{ai}(t), \hat{x}_i(t)$ and $\hat{\omega}_{i2}(t)$ signify the sensor fault estimation, actuator fault estimation, state estimation, and output noise estimation, respectively. The ith unknown input observer is created for the standardized USV dynamics as

$$\dot{z}_i(t) = (\Theta\bar{A} - J_1\bar{C})z_i(t) + \Theta\bar{B}\delta_i(t) + (J_1 + J_2)y_i(t) \tag{10}$$

where $z_i(t)$ indicates the observer state, and Θ, J_1, J_2 are invented observer gains.

Under the standardization and observer process, define $e_{i1}(t) = \bar{x}_i(t) - \hat{\bar{x}}_i(t) = [e_{xi}^T(t)\ e_{ai}^T(t)\ e_{si}^T(t)\ e_{\omega i}^T(t)]^T$ with the estimation errors $e_{xi}(t) = x_i(t) - \hat{x}_i(t)$, $e_{ai}(t) = f_{ai}(t) - \hat{f}_{ai}(t)$, $e_{si}(t) = f_{si}(t) - \hat{f}_{si}(t)$, and $e_{\omega i}(t) = \omega_{i2}(t) - \hat{\omega}_{i2}(t)$. Accordingly, the estimation error systems are procured as

$$\begin{aligned} \dot{e}_{i1}(t) &= \left(\Theta\bar{A} - J_1\bar{C}\right) e_{i1}(t) \\ &\quad + \left(\left(\Theta\bar{A} - J_1\bar{C}\right)H - J_2\right) y_i(t) + \Theta\bar{D}\bar{d}_i(t) \end{aligned} \tag{11}$$

To separate the extra output element within the dynamics of the enhanced estimation error (11), $\Theta = I_{12} - H\bar{C}$ and $J_2 = \left(\Theta\bar{A} - J_1\bar{C}\right)H = \bar{A}H - H\bar{C}\bar{A}H - J_1\bar{C}H$ are defined. Then, it follows that

$$\begin{aligned} \dot{e}_1(t) &= \left(I_N \otimes \left(\bar{A} - H\bar{C}\bar{A} - J_1\bar{C}\right)\right) e_1(t) \\ &\quad + \left(I_N \otimes \left(\bar{D} - H\bar{C}\bar{D}\right)\right) \bar{d}(t) \end{aligned} \tag{12}$$

where $e_1(t) = [e_{11}^T(t), \cdots, e_{N1}^T(t)]^T$ and the $\bar{d}(t) = [\bar{d}_1^T(t), \cdots, \bar{d}_N^T(t)]^T$.

Remark 3: Combined with effective normalization and observer design for multi-USVs, the enhanced estimation error systems (11), (12) are intuitively constructed. Simultaneous output channel noise and sensor fault estimations are further integrated into the defense-based fault-tolerant consensus tracking controller, which, in additive combination with neighboring output information, distributively compensates for sensor/actuator faults, disturbances, and noises in the physical hierarchy. The control framework of cyber-physical layers of multi-USVs is illustrated in Figure 1.

B. Defense and fault-tolerant consensus tracking design

The distributed security technique-based fault-tolerant consensus tracking controller of the ith following USV subject to connectivity-mixed attacks, as well as actuator/sensor faults,

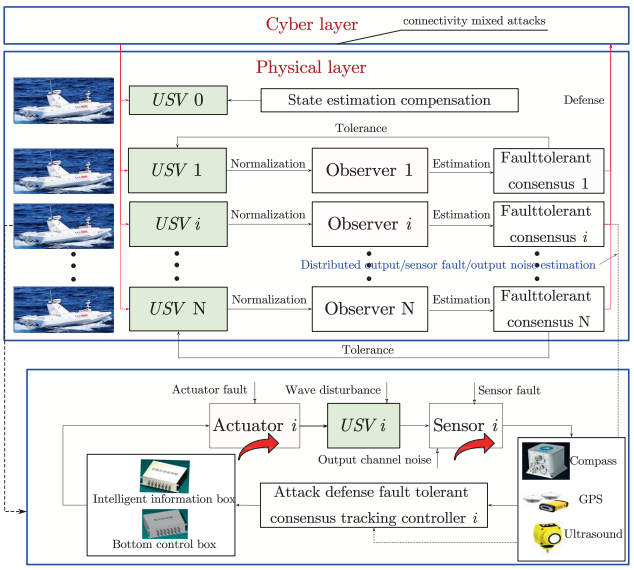

Fig. 1. Control framework of normalization/observer and defense/fault-tolerant consensus tracking control designs

wave-induced disturbances, and output noises in the cyber-physical hierarchy is designed as

$$\begin{aligned}&\delta_i(t) = -K\hat{\bar{x}}_i(t)\\&+\sigma R(\textstyle\sum_{j=1}^{N} a_{ij}^{\gamma(t)}(y_j(t)-y_i(t)) + b_i^{\gamma(t)}(y_0(t)-y_i(t)))\\&+\sigma RF_s(\textstyle\sum_{j=1}^{N} a_{ij}^{\gamma(t)}(\hat{f}_{sj}(t)-\hat{f}_{si}(t)) - b_i^{\gamma(t)}\hat{f}_{si}(t))\\&+\sigma RE_2(\textstyle\sum_{j=1}^{N} a_{ij}^{\gamma(t)}(\hat{\omega}_{j2}(t)-\hat{\omega}_{i2}(t)) - b_i^{\gamma(t)}\hat{\omega}_{i2}(t))\end{aligned} \tag{13}$$

where $K = [K_x \ K_a \ \mathbf{0}_{1\times 2} \ \mathbf{0}_{1\times 2}]$ indicates the compensation matrix with the estimation matrices K_x and the pseudo-inverse form $K_a = B^{\dagger}F_a$, R is the coupling matrix, $\sigma > 0$ is the integration coefficient, and $a_{ij}^{\gamma(t)}$ and $b_i^{\gamma(t)}$ are defined with the switching topology $\mathcal{G}_{\gamma(t)}$.

Define the leader-following consensus tracking error as $e_{i2}(t) = x_i(t) - x_0(t)$. The corresponding tracking error systems of each USV system are deduced as

$$\begin{aligned}&\dot{e}_{i2}(t) = (A-BK_x)e_{i2}(t) + BKe_{i1}(t) + E_1\omega_{i1}(t)\\&+\sigma BRC(\textstyle\sum_{j=1}^{N} a_{ij}^{\gamma(t)}(e_{j2}(t)-e_{i2}(t)) - b_i^{\gamma(t)}e_{i2}(t))\\&+\sigma BRF_s(\textstyle\sum_{j=1}^{N} a_{ij}^{\gamma(t)}(e_{sj}(t)-e_{si}(t)) - b_i^{\gamma(t)}e_{si}(t))\\&+\sigma BRE_2(\textstyle\sum_{j=1}^{N} a_{ij}^{\gamma(t)}(e_{\omega j}(t)-e_{\omega i}(t)) - b_i^{\gamma(t)}e_{\omega i}(t))\end{aligned} \tag{14}$$

Furthermore, the global leader-following consensus tracking error behavior is given as

$$\begin{aligned}&\dot{e}_2(t) = (I_N\otimes(A-BK_x) - \sigma(\mathcal{H}_{\gamma(t)}\otimes BRC))e_2(t)\\&+(I_N\otimes BK)e_1(t) + (I_N\otimes E_1)\omega_1(t)\\&-\sigma(\mathcal{H}_{\gamma(t)}\otimes BRF_s)e_s(t) - \sigma(\mathcal{H}_{\gamma(t)}\otimes BRE_2)e_\omega(t)\\&= (I_N\otimes(A-BK_x) - \sigma(\mathcal{H}_{\gamma(t)}\otimes BRC))e_2(t)\\&+(I_N\otimes E_1)\omega_1(t) + (I_N\otimes BK\\&-\sigma\mathcal{H}_{\gamma(t)}\otimes BRF_sE_s - \sigma\mathcal{H}_{\gamma(t)}\otimes BRE_2E_\omega)e_1(t)\end{aligned} \tag{15}$$

where $E_s = [\mathbf{0}_{2\times 5} \ \mathbf{0}_{2\times 3} \ I_2 \ \mathbf{0}_{2\times 2}]$, $E_\omega = [\mathbf{0}_{2\times 5} \ \mathbf{0}_{2\times 3} \ \mathbf{0}_{2\times 2} \ I_2]$, $e_2(t) = [e_{12}^T(t),\cdots,e_{N2}^T(t)]^T, \omega_1(t) = [\omega_{11}^T(t),\cdots,\omega_{N1}^T(t)]^T$, $e_s(t) = [e_{s1}^T(t),\cdots,e_{sN}^T(t)]^T, e_\omega(t) = [e_{\omega 1}^T(t),\cdots,e_{\omega N}^T(t)]^T$.

Theorem 1: Given positive constants $\chi_1,\chi_2,\chi_3,\chi_4,\sigma_\Gamma$ and σ_0, the leader-following multi-USVs (2), (5) subject to the connectivity-mixed attacks, as well as sensor/actuator faults, wave-induced disturbances, and output noises in the cyber-physical layer can achieve an exponential consensus tracking property in Definition 3 through an integrated structure of the standardization and observer mechanism (8), (10) and the defense and fault-tolerant consensus tracking control design (13) when the following two conditions are satisfied:

(1) The positive-definite symmetric matrix P, matrices K_x, H, J_1 and positive constants τ_1,τ_2,τ_3 exist such that

$$\begin{aligned}&\chi_1\left(\mathrm{He}[(A-BK_x)^TP] + E_1E_1^T\right) < \chi_1\chi_3 P\\&< \chi_3\left(\mathrm{He}[(BK_x-A)^TP] - \lambda_2\varphi_{\max}E_1E_1^T\right)\end{aligned} \tag{16}$$

$$\begin{aligned}&\tfrac{1}{\tau_1}\mathrm{He}[\bar{A} - H\bar{C}\bar{A} - J_1\bar{C}]\\&+\tfrac{1}{\tau_1}(\bar{D}-H\bar{C}\bar{D})(\bar{D}-H\bar{C}\bar{D})^T + K^TK + \chi_2 I_{12}\\&-\sigma(E_s^TF_s^TR^TRF_sE_s + E_\omega^TE_2^TR^TRE_2E_\omega) < 0\end{aligned} \tag{17}$$

$$\begin{aligned}&\max\left(\tfrac{\epsilon_a}{\chi_2} - \sqrt{\tfrac{\epsilon_a^2}{\chi_2^2} - \tfrac{\tau_2}{\chi_2}}, \tfrac{\epsilon_s}{\chi_2} - \sqrt{\tfrac{\epsilon_s^2}{\chi_2^2} - \tfrac{\tau_3}{\chi_2}}\right) < \tau_1\\&\le \min\left(\tfrac{\epsilon_a}{\chi_2} + \sqrt{\tfrac{\epsilon_a^2}{\chi_2^2} - \tfrac{\tau_2}{\chi_2}}, \tfrac{\epsilon_s}{\chi_2} + \sqrt{\tfrac{\epsilon_s^2}{\chi_2^2} - \tfrac{\tau_3}{\chi_2}}\right)\end{aligned} \tag{18}$$

$$0 < \tau_2 \le \tfrac{\epsilon_a^2}{\chi_2}, 0 < \tau_3 \le \tfrac{\epsilon_s^2}{\chi_2} \tag{19}$$

$$\max(\chi_3, \chi_4\tau_1) \ge \min(\chi_1, \chi_2\tau_1) \tag{20}$$

where the lower bounds $\underline{\epsilon}_a = \min_{\varrho=v,r,p}\epsilon_a^\varrho, \underline{\epsilon}_s = \min_{\varrho=1,2}\epsilon_s^\varrho$, $\lambda_2 = \lambda_{\max}(\Upsilon_{\gamma(t)}^2)$, and $\varphi_{\max} = \max_{i=1,\cdots,N}\varphi_{\gamma(t),i}, \gamma(t)\in\Gamma_m$.

The coupling coefficient and matrix are devised as $R = B^TP^{-1}C^{\dagger}$,$\sigma = \max\{\frac{\lambda_2}{\lambda_1+2\lambda_3}, \frac{1}{2\lambda_4(1+\lambda_4)}\}+\sigma_0$ with the preset scalar σ_0, pseudo-inverse $C^{\dagger}$, $\lambda_1 = \lambda_{\min}(\mathrm{He}[\Upsilon_{\gamma(t)}\mathcal{H}_{\gamma(t)}])$ and $\lambda_3 = \lambda_{\min}(\Upsilon_{\gamma(t)}\mathcal{H}_{\gamma(t)}\mathcal{H}_{\gamma(t)}^T\Upsilon_{\gamma(t)})$ for $\gamma(t)\in\Gamma_m$, and $\lambda_4 = \lambda_{\min}(\mathcal{H}_{\gamma(t)})$ for $\gamma(t)\in\Gamma_p$.

(2) For a decay rate $\rho_\Gamma \in (0,\rho^\star)$ with selected scalars $\rho^\star\in(0,\eta_m)$ and $\eta_m = \min(\chi_1,\chi_2\tau_1)$, the attack frequency $\mathcal{F}_\Gamma(t_0,t)$ and attack activation rates $\mathcal{R}_{\Gamma_m}(t_0,t), \mathcal{R}_{\Gamma_p}(t_0,t)$ constrain within

$$\begin{aligned}&\mathcal{F}_\Gamma(t_0,t)\\&\le \ln^{-1}\left(\tfrac{N\overline{\varphi}}{\tau_1\underline{\varphi}}((1+\tau_1)(\bar{\psi}^2+\bar{\phi}^2)+\bar{\mathcal{W}}^2)\right)(\rho^\star-\rho_\Gamma)\end{aligned} \tag{21}$$

$$\mathcal{R}_{\Gamma_m}(t_0,t) \ge \tfrac{\eta_p+\rho^\star}{\eta_m+\eta_p}, \mathcal{R}_{\Gamma_p}(t_0,t) \le \tfrac{\eta_m-\rho^\star}{\eta_m+\eta_p} \tag{22}$$

where $\eta_p = \max(\chi_3,\chi_4\tau_1), \bar{\psi} = \max_{i=1,\cdots,N}\bar{\psi}_i, \bar{\phi} = \max_{i=1,\cdots,N}\bar{\phi}_i$, $\bar{\mathcal{W}} = \max_{i=1,\cdots,N}\bar{\mathcal{W}}_i, \underline{\varphi} = \min_{i=1,\cdots,N}\varphi_{\gamma(t),i}, \overline{\varphi} = \max_{i=1,\cdots,N}\varphi_{\gamma(t),i}$, for $\gamma(t)\in\Gamma_m$.

Thus, the multi-USVs are able to fulfill the leader-following consensus tracking performance through the utilization of the subsequent exponential tracking error,

$$\|x_i(t)-x_0(t)\|^2 \le \mu_\Gamma e^{-\rho_\Gamma(t-t_0)}\|x_i(t_0)-x_0(t_0)\|^2 \tag{23}$$

with the magnitude scalar μ_Γ and decay rate ρ_Γ denoted as

$$\mu_\Gamma = \tfrac{N((1+\tau_1)(\bar{\psi}^2+\bar{\phi}^2)+\bar{\mathcal{W}}^2)(\max(\lambda_{\max}(\varphi_{\gamma(t),i}^{-1}P^{-1}),\lambda_{\max}(P^{-1}))+\sigma_\Gamma)}{\tau_1\min\left(\lambda_{\min}(\varphi_{\gamma(t),i}^{-1}P^{-1}),\lambda_{\min}(P^{-1})\right)} \tag{24}$$

Proof. Consider the piece-wise Lyapunov function $V_1(t) = V_1^m(t)$ for $\gamma(t)\in\Gamma_m$ (connectivity-maintained topologies)

and $V_1(t) = V_1^p(t)$ for $\gamma(t) \in \Gamma_p$ (connectivity-paralyzed topologies) as follows

$$\begin{cases} V_1^m(t) & = \sum_{i=1}^N e_{i2}^T(t)\varphi_{\gamma(t),i}^{-1}P^{-1}e_{i2}(t), \gamma(t) \in \Gamma_m \\ V_1^p(t) & = \sum_{i=1}^N e_{i2}^T(t)P^{-1}e_{i2}(t), \gamma(t) \in \Gamma_p \end{cases} \tag{25}$$

where P denotes a symmetric positive-defined matrix, while $\varphi_{\gamma(t),i}^{-1}, \gamma(t) \in \Gamma_m, i = 1, \cdots, N$ represents the scalar entry of the diagonal positive-definite matrix $\Phi_{\gamma(t)}$ in Lemma 1 [37].

Define the vector $\vartheta(t) = [\vartheta_1^T(t), \cdots, \vartheta_N^T(t)]^T$ with each element $\vartheta_i(t) = P^{-1}e_{i2}(t)$. According to the designed coupling matrix $R = B^TP^{-1}C^\dagger$, the derivative of the Lyapunov function $V_1^m(t)$ (25) when $\gamma(t) \in \Gamma_m$ is attained as

$$\begin{aligned} &\dot{V}_1^m = \vartheta^T(\Upsilon_{\gamma(t)} \otimes \mathrm{He}[(A - BK_x)P])\vartheta \\ &-\sigma\vartheta^T(\mathrm{He}[\Upsilon_{\gamma(t)}\mathcal{H}_{\gamma(t)}] \otimes BB^T)\vartheta + 2\sum_{i=1}^N \vartheta_i^T\varphi_{\gamma(t),i}^{-1}E_1\omega_{i1} \\ &+2\vartheta^T(\Upsilon_{\gamma(t)} \otimes BK - \sigma\Upsilon_{\gamma(t)}\mathcal{H}_{\gamma(t)} \otimes BR(F_sE_s + E_2E_\omega))e_1 \\ &\le \vartheta^T\left(\Upsilon_{\gamma(t)} \otimes \mathrm{He}\left[(A - BK_x)P\right]\right)\vartheta \\ &-\sigma\lambda_1\vartheta^T\left(I_N \otimes BB^T\right)\vartheta + \omega_1^T\omega_1 \\ &+\lambda_2\vartheta^T\left(I_N \otimes E_1E_1^T\right)\vartheta + \lambda_2\vartheta^T\left(I_N \otimes BB^T\right)\vartheta \\ &-2\sigma\lambda_3\vartheta^T(I_N \otimes BB^T)\vartheta + e_1^T(I_N \otimes (K^TK \\ &-\sigma E_s^TF_s^TR^TRF_sE_s - \sigma E_\omega^TE_2^TR^TRE_2E_\omega))e_1 \\ &\le \vartheta^T\left(\Upsilon_{\gamma(t)} \otimes \left(\mathrm{He}\left[(A - BK_x)P\right] + \lambda_2\varphi_{\max}E_1E_1^T\right)\right)\vartheta \\ &+\omega_1^T\omega_1 + e_1^T(I_N \otimes (K^TK - \sigma E_s^TF_s^TR^TRF_sE_s \\ &-\sigma E_\omega^TE_2^TR^TRE_2E_\omega))e_1 \end{aligned} \tag{26}$$

where $\sigma \ge \frac{\lambda_2}{\lambda_1+2\lambda_3}$ with $\lambda_1 = \lambda_{\min}(\mathrm{He}[\Upsilon_{\gamma(t)}\mathcal{H}_{\gamma(t)}]), \lambda_2 = \lambda_{\max}(\Upsilon_{\gamma(t)}^2)$ and $\lambda_3 = \lambda_{\min}(\Upsilon_{\gamma(t)}\mathcal{H}_{\gamma(t)}\mathcal{H}_{\gamma(t)}^T\Upsilon_{\gamma(t)})$, and $\varphi_{\max} = \max_{i=1,\cdots,N}\varphi_{\gamma(t),i}, \gamma(t) \in \Gamma_m$.

Subsequently, the derivative of $V_1^p(t)$ (25) when $\gamma(t) \in \Gamma_p$ is achieved as

$$\begin{aligned} &\dot{V}_1^p \le \vartheta^T\left(I_N \otimes \mathrm{He}\left[(A - BK_x)P\right]\right)\vartheta \\ &+\vartheta^T\left(I_N \otimes E_1E_1^T\right)\vartheta + \omega_1^T\omega_1 \\ &-2\sigma\vartheta^T(\mathcal{H}_{\gamma(t)} \otimes BB^T)\vartheta + \vartheta^T\left(I_N \otimes BB^T\right)\vartheta \\ &+e_1^T\left(I_N \otimes K^TK\right)e_1 - 2\sigma\vartheta^T(\mathcal{H}_{\gamma(t)}\mathcal{H}_{\gamma(t)}^T \otimes BB^T)\vartheta \\ &-\sigma e_1^T\left(I_N \otimes E_s^TF_s^TR^TRF_sE_s\right)e_1 \\ &-\sigma e_1^T\left(I_N \otimes E_\omega^TE_2^TR^TRE_2E_\omega\right)e_1 \\ &\le \vartheta^T\left(I_N \otimes \mathrm{He}\left[(A - BK_x)P\right]\right)\vartheta \\ &+\vartheta^T\left(I_N \otimes E_1E_1^T\right)\vartheta + \omega_1^T\omega_1 \\ &+\left(-2\sigma\lambda_4 - 2\sigma\lambda_4^2 + 1\right)\vartheta^T(I_N \otimes BB^T)\vartheta \\ &+e_1^T(I_N \otimes (K^TK - \sigma E_s^TF_s^TR^TRF_sE_s \\ &-\sigma E_\omega^TE_2^TR^TRE_2E_\omega))e_1 \\ &\le \vartheta^T\left(I_N \otimes \left(\mathrm{He}\left[(A - BK_x)P\right] + E_1E_1^T\right)\right)\vartheta \\ &+\omega_1^T\omega_1 + e_1^T(I_N \otimes (K^TK - \sigma E_s^TF_s^TR^TRF_sE_s \\ &-\sigma E_\omega^TE_2^TR^TRE_2E_\omega))e_1 \end{aligned} \tag{27}$$

where $\sigma \ge \frac{1}{2\lambda_4(1+\lambda_4)}$ with $\lambda_4 = \lambda_{\min}(\mathcal{H}_{\gamma(t)}), \gamma(t) \in \Gamma_p$.

Take into account an alternative Lyapunov function $V_2(t)$ with the combination of $e_{i1}(t)$ and the derivative type of the unified sensor and actuator faults as follows

$$\begin{aligned} V_2(t) & = \sum_{i=1}^N(\tfrac{1}{\tau_1}e_{i1}^T(t)e_{i1}(t) \\ & \quad +\tfrac{1}{\tau_2}\dot{f}_{ai}^T(t)\dot{f}_{ai}(t) + \tfrac{1}{\tau_3}\dot{f}_{si}^T(t)\dot{f}_{si}(t)) \end{aligned} \tag{28}$$

where $\tau_1 > 0, \tau_2 > 0$ and $\tau_3 > 0$.

Prior to computing the derivative of $V_2(t)$, the connection of the first-/second-order derivatives of abrupt-/incipient-type sensor/actuator faults $f_{\delta i}^\varrho(t), \varrho = v, r, p$ and $f_{si}^\varrho(t), \varrho = 1, 2$ in [3] are modeled as exponentially varying properties,

$$\ddot{f}_{\delta i}^\varrho(t) = -\epsilon_a^\varrho\dot{f}_{\delta i}^\varrho(t), \ddot{f}_{si}^\varrho(t) = -\epsilon_s^\varrho\dot{f}_{si}^\varrho(t) \tag{29}$$

Subsequently, the derivative of $V_2(t)$ (28) is acquired as

$$\begin{aligned} &\dot{V}_2 \le \tfrac{1}{\tau_1}\sum_{i=1}^N e_{i1}^T\mathrm{He}[\bar{A} - H\bar{C}\bar{A} - J_1\bar{C}] \\ &+(\bar{D} - H\bar{C}\bar{D})(\bar{D} - H\bar{C}\bar{D})^T)e_{i1} \\ &+\tfrac{1}{\tau_1}\sum_{i=1}^N\left(\omega_{i1}^T\omega_{i1} + \dot{\omega}_{i2}^T\dot{\omega}_{i2}\right) \\ &+\sum_{i=1}^N((\tfrac{1}{\tau_1} - \tfrac{2\underline{\epsilon}_a}{\tau_2})\dot{f}_{ai}^T\dot{f}_{ai} + (\tfrac{1}{\tau_1} - \tfrac{2\underline{\epsilon}_s}{\tau_3})\dot{f}_{si}^T\dot{f}_{si}) \end{aligned} \tag{30}$$

where $\underline{\epsilon}_a = \min_{\varrho=v,r,p}\epsilon_a^\varrho$ and $\underline{\epsilon}_s = \min_{\varrho=1,2}\epsilon_s^\varrho$.

According to (16), $\mathrm{He}\left[(A - BK_x)P\right] + \lambda_2\varphi_{\max}E_1E_1^T + \chi_1P < 0$ is derived with the selected scalar $\chi_1 > 0$. Applying the inequality constraint $\frac{1}{\tau_1}(\mathrm{He}[\bar{A} - H\bar{C}\bar{A} - J_1\bar{C}] + (\bar{D} - H\bar{C}\bar{D})(\bar{D} - H\bar{C}\bar{D})^T) + K^TK - \sigma(E_s^TF_s^TR^TRF_sE_s + E_\omega^TE_2^TR^TRE_2E_\omega) + \chi_2I_{12} < 0$ in (17), the derivative of $V_1^m(t)+V_2(t)$ when $\gamma(t) \in \Gamma_m$ under connectivity-maintained topologies is obtained as

$$\begin{aligned} &\dot{V}_1^m(t) + \dot{V}_2(t) < -\chi_1V_1^m(t) - \chi_2\tau_1V_2(t) \\ &+\tfrac{1+\tau_1}{\tau_1}\omega_1^T(t)\omega_1(t) + \tfrac{1}{\tau_1}\dot{\omega}_2^T(t)\dot{\omega}_2(t) \\ &+\sum_{i=1}^N\left(\tfrac{\chi_2\tau_1 - 2\underline{\epsilon}_a}{\tau_2} + \tfrac{1}{\tau_1}\right)\dot{f}_{ai}^T(t)\dot{f}_{ai}(t) \\ &+\sum_{i=1}^N\left(\tfrac{\chi_2\tau_1 - 2\underline{\epsilon}_s}{\tau_3} + \tfrac{1}{\tau_1}\right)\dot{f}_{si}^T(t)\dot{f}_{si}(t) \\ &\le -\min\left(\chi_1, \chi_2\tau_1\right)\left(V_1^m(t) + V_2(t)\right) \\ &+\tfrac{1+\tau_1}{\tau_1}\omega_1^T(t)\omega_1(t) + \tfrac{1}{\tau_1}\dot{\omega}_2^T(t)\dot{\omega}_2(t) \end{aligned} \tag{31}$$

where $\frac{\chi_2\tau_1}{\tau_2} + \frac{1}{\tau_1} - \frac{2\underline{\epsilon}_a}{\tau_2} \le 0$ and $\frac{\chi_2\tau_1}{\tau_3} + \frac{1}{\tau_1} - \frac{2\underline{\epsilon}_s}{\tau_3} \le 0$ are obtained in accordance with the scalar limitations (18), (19) with the chosen $\chi_2 > 0$.

In the meantime, according to (16), $\mathrm{He}\left[(A - BK_x)P\right] + E_1E_1^T - \chi_3P < 0$ is provided with the selected scalar $\chi_3 > 0$. Complying with $\frac{1}{\tau_1}(\mathrm{He}[\bar{A} - H\bar{C}\bar{A} - J_1\bar{C}] + (\bar{D} - H\bar{C}\bar{D})(\bar{D} - H\bar{C}\bar{D})^T) + K^TK - \sigma(E_s^TF_s^TR^TRF_sE_s + E_\omega^TE_2^TR^TRE_2E_\omega) - \chi_4I_{12} < 0$ in (17), the derivative of $V_1^p(t) + V_2(t)$ when $\gamma(t) \in \Gamma_p$ is attained as

$$\begin{aligned} &\dot{V}_1^p(t) + \dot{V}_2(t) \le \max\left(\chi_3, \chi_4\tau_1\right)\left(V_1^p(t) + V_2(t)\right) \\ &+\tfrac{1+\tau_1}{\tau_1}\omega_1^T(t)\omega_1(t) + \tfrac{1}{\tau_1}\dot{\omega}_2^T(t)\dot{\omega}_2(t) \end{aligned} \tag{32}$$

where $\chi_4 > 0$, $-\frac{\chi_4\tau_1}{\tau_2} + \frac{1}{\tau_1} - \frac{2\underline{\epsilon}_a}{\tau_2} \le 0$ and $-\frac{\chi_4\tau_1}{\tau_3} + \frac{1}{\tau_1} - \frac{2\underline{\epsilon}_s}{\tau_3} \le 0$ are also derived in (18), (19).

Finally, give the total Lyapunov characterization

$$V(t, \gamma(t)) = \begin{cases} V_1^m(t) + V_2(t), \gamma(t) \in \Gamma_m \\ V_1^p(t) + V_2(t), \gamma(t) \in \Gamma_p \end{cases} \tag{33}$$

According to $\max(\chi_3, \chi_4\tau_1) \ge \min(\chi_1, \chi_2\tau_1)$ in (20), for $\gamma(t) \in \Gamma = \Gamma_m \cup \Gamma_p$, it is derived with integrating both sides of $\dot{V}(t, \gamma(t))$ over $t \in [t_k, t_{k+1})$,

$$V(t, \gamma(t)) < \xi e^{\eta_pT_p(t_k,t) - \eta_mT_m(t_k,t)}V(t_k, \gamma(t_k)) \tag{34}$$

where $\eta_p = \max(\chi_3, \chi_4\tau_1), \eta_m = \min(\chi_1, \chi_2\tau_1)$ and $\xi = \frac{N}{\tau_1}((1 + \tau_1)(\bar{\psi}^2 + \bar{\phi}^2) + \bar{\mathcal{W}}^2)$ with $\bar{\psi} = \max_{i=1,\cdots,N}\bar{\psi}_i, \bar{\phi} = \max_{i=1,\cdots,N}\bar{\phi}_i, \bar{\mathcal{W}} = \max_{i=1,\cdots,N}\bar{\mathcal{W}}_i$, and $T_m(t_k, t), T_p(t_k, t)$ exhibit the total activation time in Definition 2 [33].

Since $\underline{\varphi}V_1^m(t) \le \sum_{i=1}^N e_{i2}^T(t)P^{-1}e_{i2}(t) \le \overline{\varphi}V_1^m(t)$ is generated with $\underline{\varphi} = \min_{i=1,\cdots,N}\varphi_{\gamma(t),i}, \overline{\varphi} = \max_{i=1,\cdots,N}\varphi_{\gamma(t),i}$ when

$\gamma(t) \in \Gamma_m$, $V(t_k, \gamma(t_k)) \leq \frac{\overline{\varphi}}{\underline{\varphi}} V(t_k^-, \gamma(t_k^-))$ is subsequently obtained at every switching event $t_k, k \in \mathbb{N}$.

Successively, it is determined that

$$\begin{aligned} &V(t,\gamma(t)) < \xi e^{\eta_p T_p(t_k,t)-\eta_m T_m(t_k,t)} \frac{\overline{\varphi}}{\underline{\varphi}} V(t_k^-, \gamma(t_k^-)) \\ &< \xi^2 e^{\eta_p T_p(t_{k-1},t)-\eta_m T_m(t_{k-1},t)} \frac{\overline{\varphi}}{\underline{\varphi}} V(t_{k-1}, \gamma(t_{k-1})) \\ &< \cdots < \xi^{k+1} e^{\eta_p T_p(t_0,t)-\eta_m T_m(t_0,t)} \left(\frac{\overline{\varphi}}{\underline{\varphi}}\right)^k V(t_0,\gamma(t_0)) \\ &= \xi e^{N_\Gamma(t_0,t)\ln\left(\frac{\xi\overline{\varphi}}{\underline{\varphi}}\right)+\eta_p T_p(t_0,t)-\eta_m T_m(t_0,t)} V(t_0,\gamma(t_0)) \end{aligned} \tag{35}$$

where k is denoted by the attack number, i.e., $k = N_\Gamma(t_0,t)$ in Definition 1 [33].

Since the attack frequency $\mathcal{F}_\Gamma(t_0,t)$ in Definition 1 is satisfied in (21), $N_\Gamma(t_0,t)\ln(\frac{\xi\overline{\varphi}}{\underline{\varphi}}) \leq (\rho^\star - \rho_\Gamma)(t-t_0)$ is then garnered. $\eta_p T_p(t_0,t) - \eta_m T_m(t_0,t) \leq -\rho^\star(t-t_0)$ is inferred from the connectivity-maintained/-paralyzed attack activation rates $\mathcal{R}_{\Gamma_m}(t_0,t)$ and $\mathcal{R}_{\Gamma_p}(t_0,t)$ (22) in Definition 2. Then, $N_\Gamma(t_0,t)\ln(\frac{\xi\overline{\varphi}}{\underline{\varphi}}) + \eta_p T_p(t_0,t) - \eta_m T_m(t_0,t) \leq -\rho_\Gamma(t-t_0)$ is attained, and therefore it can be deduced that,

$$V(t,\gamma(t)) < \xi e^{-\rho_\Gamma(t-t_0)} V(t_0,\gamma(t_0)) \tag{36}$$

The total Lyapunov candidate at the initial time instant t_0, denoted by $V(t,\gamma(t)), \gamma(t) \in \Gamma$, can be expressed follows

$$\begin{aligned} &V(t_0,\gamma(t_0)) \\ &\leq \max\left(\lambda_{\max}(\varphi_{\gamma(t),i}^{-1}P^{-1}), \lambda_{\max}(P^{-1})\right)\sum_{i=1}^N \|e_{i2}(t_0)\|^2 + \\ &\frac{\max\limits_{i=1,\cdots,N}(\frac{1}{\tau_1}\|e_{i1}(t_0)\|^2+\frac{1}{\tau_2}\|\dot{f}_{ai}(t_0)\|^2+\frac{1}{\tau_3}\|\dot{f}_{si}(t_0)\|^2)}{\min\limits_{i=1,\cdots,N}\|e_{i2}(t_0)\|^2}\sum_{i=1}^N \|e_{i2}(t_0)\|^2 \end{aligned} \tag{37}$$

Denote $\Lambda_\Gamma = \max(\lambda_{\max}(\varphi_{\gamma(t),i}^{-1}P^{-1}), \lambda_{\max}(P^{-1})) + \sigma_\Gamma$ for $\gamma(t) \in \Gamma_m$ with the specified constant $\sigma_\Gamma > 0$, it follows that

$$\begin{aligned} &\min\left(\lambda_{\min}(\varphi_{\gamma(t),i}^{-1}P^{-1}), \lambda_{\min}(P^{-1})\right)\sum_{i=1}^N \|e_{i2}(t)\|^2 \\ &\leq V(t,\gamma(t)) < \xi e^{-\rho_\Gamma(t-t_0)} V(t_0,\gamma(t_0)) \\ &\leq \xi\Lambda_\Gamma e^{-\rho_\Gamma(t-t_0)}\sum_{i=1}^N \|e_{i2}(t_0)\|^2 \end{aligned} \tag{38}$$

and the leader-following consensus tracking error in Definition 3 yields that

$$\begin{aligned} &\|x_i(t) - x_0(t)\|^2 \leq \frac{\xi\Lambda_\Gamma e^{-\rho_\Gamma(t-t_0)}\|e_{i2}(t_0)\|^2}{\min\left(\lambda_{\min}(\varphi_{\gamma(t),i}^{-1}P^{-1}), \lambda_{\min}(P^{-1})\right)} \\ &= \mu_\Gamma e^{-\rho_\Gamma(t-t_0)}\|x_i(t_0) - x_0(t_0)\|^2 \end{aligned} \tag{39}$$

with μ_Γ expressed in (24). □

Remark 4: The consensus tracking objective of the leader-following multi-USVs is achieved through three crucial strategies: robust compensation for faults in actuators and sensors, resilience against mixed attacks, and utilization of the interaction-based output data, estimated output noises, and sensor faults to improve the convergence of tracking performance. Additionally, exponential error margins are derived to measure the impact of hostile attacks, wherein the decay rate and amplitude are influenced by the agent quantity (N) and the upper limit of input/output noises.

Remark 5: (i) Specific mixed attacks can be effectively defended against by setting feasible threshold functions (21) and (22) for activation rates $\mathcal{R}_{\Gamma_m}(t_0,t), \mathcal{R}_{\Gamma_p}(t_0,t)$ and attack frequency $\mathcal{F}_\Gamma(t_0,t)$. (ii) The bilinear nature of the nonlinear matrix inequality (17) leads to a complex and tedious solution. By utilizing parametric matrix decomposability and applying Schur's Lemma, the inequality can be effectively solved by means of a multidimensional and readily established linear matrix inequality (40), where $\Omega_{12} = \frac{1}{\tau_1}(F_a - H_1CF_a - A^TC^TH_2^T - C^TJ_{12}^T) + K_x^TK_a, \Omega_{13} = -\frac{1}{\tau_1}(J_{11}F_s + A^TC^TH_3^T + C^TJ_{13}^T), \Omega_{14} = -\frac{1}{\tau_1}(J_{11}E_2 + A^TC^TH_4^T + C^TJ_{14}^T), \Omega_{22} = -\frac{1}{\tau_1}\mathrm{He}[H_2CF_a] + K_a^TK_a + \chi_2 I_3, \Omega_{23} = -\frac{1}{\tau_1}(J_{12}F_s + F_a^TC^TH_3^T), \Omega_{24} = -\frac{1}{\tau_1}(J_{12}E_2 + F_a^TC^TH_4^T), \Omega_{33} = -\frac{1}{\tau_1}\mathrm{He}[J_{13}F_s] + \chi_2 I_2 - \sigma F_s^TR^TRF_s, \Omega_{34} = -\frac{1}{\tau_1}(J_{13}E_2 + F_s^TJ_{14}^T)$, and $\Omega_{44} = -\frac{1}{\tau_1}\mathrm{He}[J_{14}E_2] - \sigma E_2^TR^TRE_2 + \chi_2 I_2$ with block decoupling matrices $H = [H_1^T\ H_2^T\ H_3^T\ H_4^T]^T, J_1 = [J_{11}^T\ J_{12}^T\ J_{13}^T\ J_{14}^T]^T$.

IV. Simulation Results

A network of one leading USV and five following USVs with the existence of sensor and actuator faults, wave-induced disturbances, and output noises, as well as connectivity-mixed attacks is illustrated in the cyber-physical hierarchy. Comparative simulations of multi-USVs with low-forward-speed multi-topology-switching (LFS-MTS) and high-forward-speed less-topology-switching (HFS-LTS) are proposed to confirm the validity and advantage of the proposed defense and tolerance technique.

The values of parameters [17] in the sway, yaw, and roll motions of each USV under LFS-MTS and HFS-LTS scenarios are illustrated in Table I. The wave-induced disturbances are set as $\omega_{\psi i} = 0.0722\sin 0.1t - 0.0537\cos 0.1t$ and $\omega_{\phi i} = 2.028\sin 10t - 0.6478\cos 10t$ with upper bounds $\bar{\psi} = 0.0537, \bar{\phi} = 0.6477$. The output channel noises are set as the uniform distributed random noises (amplitude: $[-0.05, 0.05]$

$$\begin{bmatrix} \frac{1}{\tau_1}\mathrm{He}[A - H_1CA - J_{11}C] + K_x^TK_x + \chi_2 I_5 & \Omega_{12} & \Omega_{13} & \Omega_{14} & E_1 - H_1CE_1 & \mathbf{0}_{5\times3} & -H_1F_s & -H_1E_2 \\ \star & \Omega_{22} & \Omega_{23} & \Omega_{24} & -H_2CE_1 & I_3 & -H_2F_s & -H_2E_2 \\ \star & \star & \Omega_{33} & \Omega_{34} & -H_3CE_1 & \mathbf{0}_{2\times3} & I_2 - H_3F_s & -H_3E_2 \\ \star & \star & \star & \Omega_{44} & -H_4CE_1 & \mathbf{0}_{2\times3} & -H_4F_s & I_2 - H_4E_2 \\ \star & \star & \star & \star & -\tau_1 I_5 & \mathbf{0}_{5\times3} & \mathbf{0}_{5\times2} & \mathbf{0}_{5\times2} \\ \star & \star & \star & \star & \star & -\tau_1 I_3 & \mathbf{0}_{3\times2} & \mathbf{0}_{3\times2} \\ \star & \star & \star & \star & \star & \star & -\tau_1 I_2 & \mathbf{0}_{2\times2} \\ \star & \star & \star & \star & \star & \star & \star & -\tau_1 I_2 \end{bmatrix} < 0 \tag{40}$$

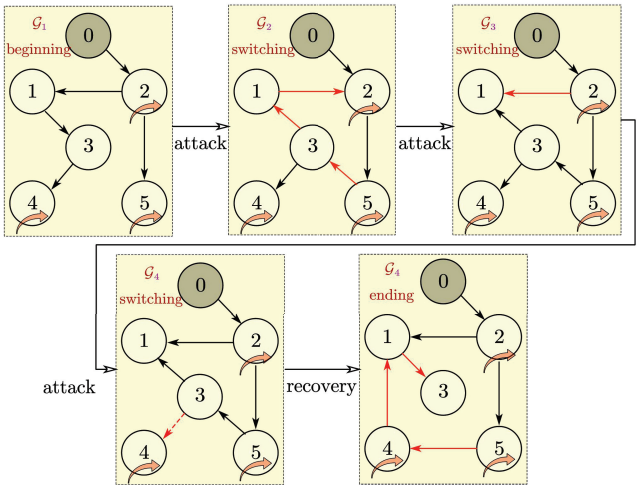

Fig. 2. LFS-MTS under connectivity-mixed attacks $\mathcal{G}_1, \cdots, \mathcal{G}_4$

and sample time: 0.1). The unified sensor/actuator faults $f_{\delta i}^{\varrho}(t), \varrho = v, r, p$ and $f_{si}^{\varrho}(t), \varrho = 1, 2$ are set as

$$
\begin{aligned}
f_{\delta 4}^{\varrho}(t) &= \begin{cases} 0.5(1-e^{-0.5t}), 0 \le t < 10 \\ 0.001(1-e^{-0.05t}), 10 \le t \le 80 \end{cases} \\
f_{\delta 2}^{\varrho}(t) &= \begin{cases} -(1-e^{-0.05t}), 0 \le t < 20 \\ -2(1-e^{-0.05t}), 20 \le t \le 80 \end{cases} \\
f_{s5}^{\varrho}(t) &= \begin{cases} 1-e^{-0.05t}, 0 \le t < 70 \\ 2(1-e^{-0.05t}), 70 \le t \le 80 \end{cases}
\end{aligned} \tag{41}
$$

where the decay rate limits are fixed as $\overline{\epsilon}_{a(s)} = 0.1$ and $\underline{\epsilon}_{a(s)} = 0.005$.

Both LFS-MTS and HFS-LTS scenarios of multi-USVs under mixed attacks are identified, where the maintained and paralyzed topologies activate at each switching occurrence instant, i.e., 20s, 40s and 60s under LFS-MTS scenario in Figure 2 ($\mathcal{G}_1, \cdots, \mathcal{G}_4$) and 40s under HFS-LTS scenario in Figure 3 ($\mathcal{G}_1, \mathcal{G}_2$).

TABLE I
THE VALUES OF PARAMETERS OF THE NETWORKED USV

LFS-MTS	HFS-LTS
$U = 3.8\text{m.s}^{-1}$	$U = 7.8\text{m.s}^{-1}$
$T_v = 2/U, T_r = 1.6/U$	$T_v = 1.8/U, T_r = 2/U$
$K_{dr} = -0.0027U$	$K_{dr} = -0.0036U$
$K_{dp} = -0.0014U^2$	$K_{dp} = -0.0022U^2$
$K_{dv} = 0.01U, K_{vp} = 0.21U$	$K_{dv} = 0.06U, K_{vp} = 0.16U$
$K_{vr} = -0.46\text{m.s}^{-1}$	$K_{vr} = -0.58\text{m.s}^{-1}$
$\omega_n = 1.63\text{rad.s}^{-1}$	$\omega_n = 2.2\text{rad.s}^{-1}$
$\zeta = 0.64 + 0.38U$	$\zeta = 0.58 + 0.67U$

Figure 4 illustrates the leader-following sway velocity tracking, yaw velocity tracking, yaw angle tracking, roll velocity tracking, and roll angle tracking properties in the LFS-MTS case. It also shows the ratings and estimates of the abrupt/incipient actuator faults at 10s and 20s for USV4 and USV2, as well as the incipient sensor fault at 70s for USV5. Due to the low-speed maneuvering of multi-USVs, even though connectivity-maintained topology switching occurs at 20s, 40s and 60s under hostile attacks, it is shown by the convergence of the unidirectional fluctuations of USV2, USV4

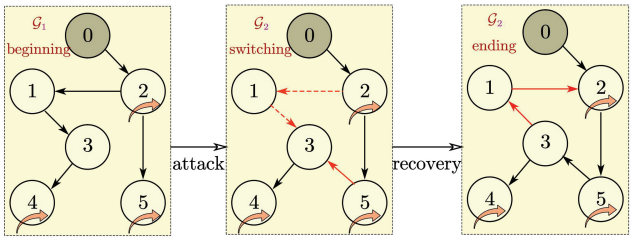

Fig. 3. HFS-LTS under connectivity-mixed attacks $\mathcal{G}_1, \mathcal{G}_2$

at 20s and the bidirectional fluctuations of USV1, USV3, and USV5 at 40s and 60s. The convergence of error terms for different USVs is represented by curves of different colors. In subplots (a), (b), (d), and (e) of Figure 4, it is evident that the blue solid line representing USV1 and the black dashed line representing USV3 show higher peaks and require more time to achieve convergence after being subjected to attacks. Figure 5 shows the effective convergence of the leader-following consensus tracking errors for multi-USVs in the HFS-LTS case and the effective tracking evaluation of USV4, USV2, and USV5 under the same compound fault action. Compared to the LFS-MTS case in Figure 4, the effect of the uniform distributed random noises is more pronounced in the HFS-LTS case. This excites more burrs on the consensus tracking errors. Additionally, at 40s, due to connectivity-mixed attacks, USV1 and USV3 require more time to converge after the attacks under the repair mechanism. This ultimately produces bidirectional fluctuations in the convergence process. Furthermore, the unified actuator failure acting on USV4 at 10s also results in poorer estimation due to random oscillations of noises and disturbances during high-speed maneuverability.

Figure 6 illustrates the impact of the proposed defense and tolerance technique based on attack frequency and activation rate index versus the consensus tracking method based on ADT index [33] on the leader-following consensus tracking errors in five-channel multi-USVs. The results clearly show that our previous work [33], which solely relies on the ADT index, fails to adequately compensate for sensor/actuator faults and protect against mixed attacks for the LFS-MTS case. Particularly, after multiple topology switches, significant deviations in consensus tracking errors, and even linear and exponential divergence occur at 60s. Figure 7 demonstrates the strong convergence effect of the proposed defense and tolerance technique, based only on the dual-index, in combating cyber-physical threats, compared to using multiple indicators (combined dual-index and ADT). Remarkably, the effective combination of the proposed dual indexes and the ADT method offers advantages in terms of both fluctuation amplitude and effective convergence time. However, limitations still exist in the LFS-MTS case. Specifically, fewer topology switches (maximum recurrence of the original topology) are required to establish a strong correlation for the defense and tolerance technique based on the activation rate and attack frequency indexes.

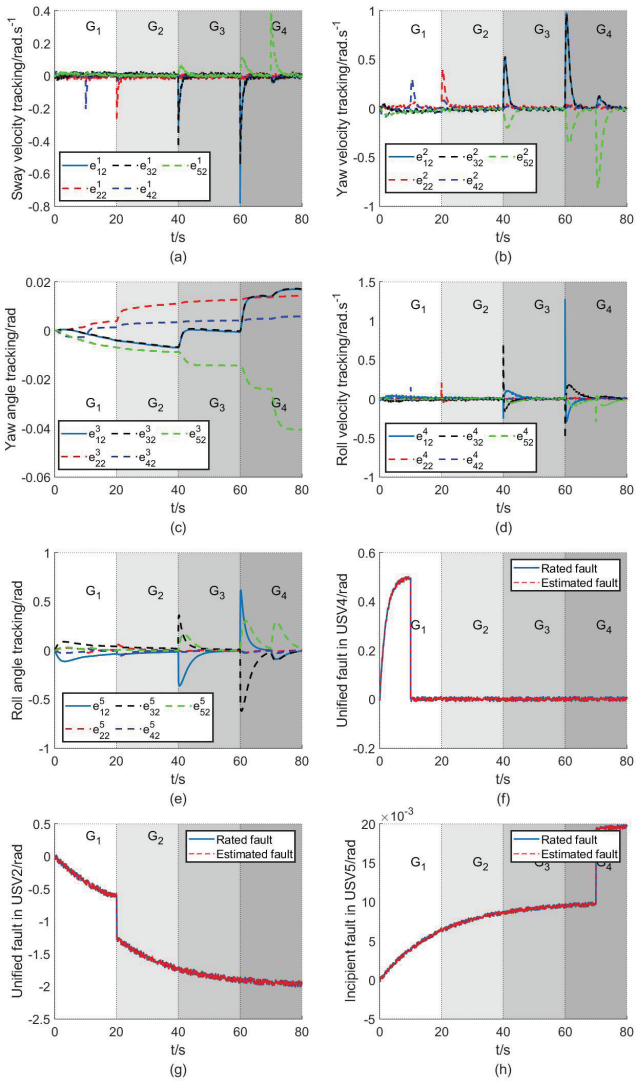

Fig. 4. Leader-following consensus tracking errors of multi-USVs and rated/estimated faults under LFS-MTS

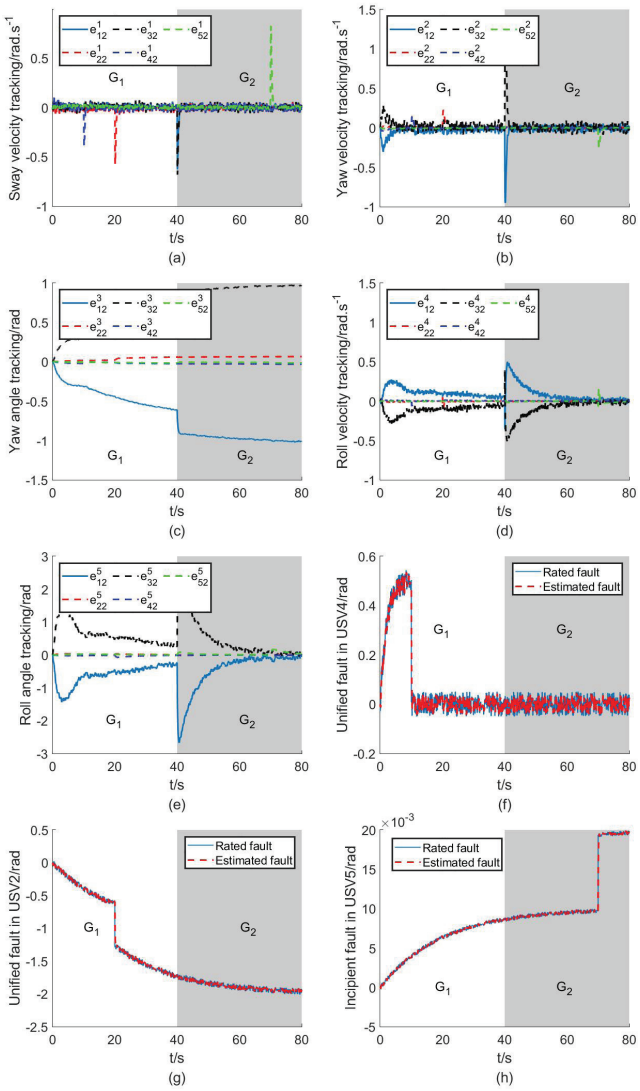

Fig. 5. Leader-following consensus tracking errors of multi-USVs and rated/estimated faults under HFS-LTS

V. Conclusions

This study presents a novel defense and tolerance technique that integrates standardization and observer, and fault-tolerant consensus tracking control protocols. The aim is to effectively mitigate cyber-physical threats faced by multi-USVs in the leader-following structure. These threats include adverse deflection caused by incipient and abrupt sensor/actuator faults, disturbances induced by waves, noise affecting the output channels, and topological switching features arising from hostile attacks. Adequate criteria are presented to build a bridge in quantitative dependence between advised leader-following exponential consensus tracking capability and dual activation rate and attack frequency indicators. Simulation results for various configurations (ADT-only, dual-index-only, and combined dual-index and ADT) demonstrate the efficiency, advantage, and economy of the defense and tolerance algorithm in leader-following USVs. Future work of realistic modeling of nonlinear multi-USVs towards defensive and tolerant competencies in mitigating physical deficiencies and the challenges posed by replay and disruptive attacks are highlighted, especially with an event-triggered mechanism of USV task execution for a substantial reduction in computational communication resources.

References

[1] Z. Liu, Y. Zhang, X. Yu, and C. Yuan, "Unmanned surface vehicles: An overview of developments and challenges," *Annual Reviews in Control*, vol. 41, pp. 71–93, 2016.

[2] H. R. Karimi and Y. Lu, "Guidance and control methodologies for marine vehicles: A survey," *Control Engineering Practice*, vol. 111, p. 104785, 2021.

[3] Z.-Q. Liu, Y.-L. Wang, and T.-B. Wang, "Incremental predictive control-based output consensus of networked unmanned surface vehicle formation systems," *Information Sciences*, vol. 457, pp. 166–181, 2018.

[4] Z. Peng, L. Liu, and J. Wang, "Output-feedback flocking control of multiple autonomous surface vehicles based on data-driven adaptive extended state observers," *IEEE Transactions on Cybernetics*, vol. 51, no. 9, pp. 4611–4622, 2021.

[5] Y. Zhao, X. Qi, Y. Ma, Z. Li, R. Malekian, and M. A. Sotelo, "Path following optimization for an underactuated usv using smoothly-convergent deep reinforcement learning," *IEEE Transactions on Intelligent Transportation Systems*, vol. 22, no. 10, pp. 6208–6220, 2021.

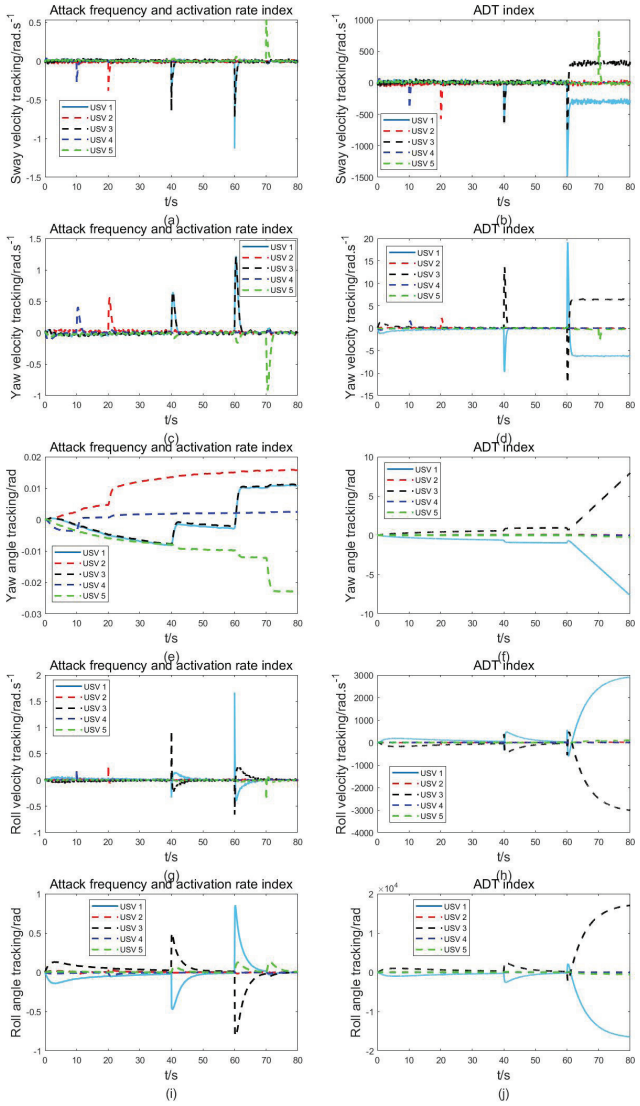

Fig. 6. Comparative analysis under LFS-MTS of the proposed attack frequency and activation rate index and ADT-only index in [33]

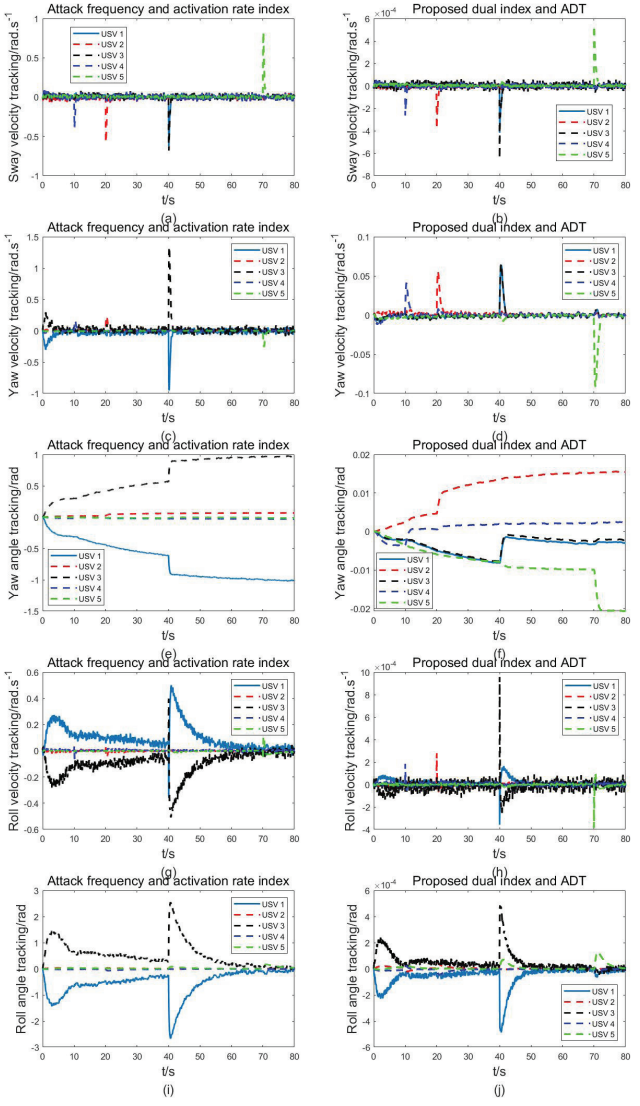

Fig. 7. Comparative analysis under HFS-LTS of the proposed attack frequency and activation rate index and proposed dual-index with combined ADT in [33]

[6] X. Sun, G. Wang, Y. Fan, D. Mu, and B. Qiu, "A formation autonomous navigation system for unmanned surface vehicles with distributed control strategy," *IEEE Transactions on Intelligent Transportation Systems*, vol. 22, no. 5, pp. 2834–2845, 2021.

[7] N. Gu, D. Wang, Z. Peng, and L. Liu, "Adaptive bounded neural network control for coordinated path-following of networked underactuated autonomous surface vehicles under time-varying state-dependent cyber-attack," *ISA transactions*, vol. 104, pp. 212–221, 2020.

[8] L. Li, Y. Tuo, T. Li, M. Tong, and S. Wang, "Time-varying formation control of multiple unmanned surface vessels with heterogeneous hydrodynamics subject to actuator attacks," *Applied Mathematics and Computation*, vol. 422, p. 126987, 2022.

[9] Z. Ye, D. Zhang, and Z.-G. Wu, "Adaptive event-based tracking control of unmanned marine vehicle systems with dos attack," *Journal of the Franklin Institute*, vol. 358, no. 3, pp. 1915–1939, 2021.

[10] D. Zhang, Z. Ye, G. Feng, and H. Li, "Intelligent event-based fuzzy dynamic positioning control of nonlinear unmanned marine vehicles under dos attack," *IEEE Transactions on Cybernetics*, 2021.

[11] Q. Zhong, S. Han, K. Shi, X. Cai, O.-M. Kwon, and S. Zhong, "Secure consensus switching control for multiagent system under abnormal deception attacks and its application to unmanned surface vehicle clusters," *Expert Systems with Applications*, p. 117702, 2022.

[12] Z. Ye, D. Zhang, Z.-G. Wu, and H. Yan, "A3c-based intelligent event-triggering control of networked nonlinear unmanned marine vehicles subject to hybrid attacks," *IEEE Transactions on Intelligent Transportation Systems*, 2021.

[13] Z. Feng, G. Hu, and G. Wen, "Distributed consensus tracking for multi-agent systems under two types of attacks," *International Journal of Robust and Nonlinear Control*, vol. 26, no. 5, pp. 896–918, 2016.

[14] G. Zhang, S. Chu, J. Huang, and W. Zhang, "Robust adaptive fault-tolerant control for unmanned surface vehicle via the multiplied event-triggered mechanism," *Ocean Engineering*, vol. 249, p. 110755, 2022.

[15] J. Zhang, S. Yu, and Y. Yan, "Fixed-time velocity-free sliding mode tracking control for marine surface vessels with uncertainties and unknown actuator faults," *Ocean Engineering*, vol. 201, p. 107107, 2020.

[16] C. Zhang, C. Cao, C. Guo, T. Li, and M. Guo, "Navigation multisensor fault diagnosis approach for an unmanned surface vessel adopted particle-filter method," *IEEE Sensors Journal*, vol. 21, no. 23, pp. 27 093–27 105, 2021.

[17] Y.-L. Wang and Q.-L. Han, "Network-based fault detection filter and controller coordinated design for unmanned surface vehicles in network environments," *IEEE Transactions on Industrial Informatics*, vol. 12, no. 5, pp. 1753–1765, 2016.

[18] X. Wang, Z. Fei, H. Gao, and J. Yu, "Integral-based event-triggered fault detection filter design for unmanned surface vehicles," *IEEE Transactions on Industrial Informatics*, vol. 15, no. 10, pp. 5626–5636, 2019.

[19] L. Chen, M. Liu, Y. Shi, H. Zhang, and E. Zhao, "Adaptive fault estimation for unmanned surface vessels with a neural network observer

approach," *IEEE Transactions on Circuits and Systems I: Regular Papers*, vol. 68, no. 1, pp. 416–425, 2021.
[20] K. Zhu and Y. Wang, "Event-triggered sensor fault estimation of unreliable networked unmanned surface vehicle system with correlated noises," *IEEE Transactions on Vehicular Technology*, vol. 71, no. 3, pp. 2527–2537, 2022.
[21] X. Jin, "Fault tolerant finite-time leader–follower formation control for autonomous surface vessels with los range and angle constraints," *Automatica*, vol. 68, pp. 228–236, 2016.
[22] J.-X. Zhang and G.-H. Yang, "Fault-tolerant leader-follower formation control of marine surface vessels with unknown dynamics and actuator faults," *International Journal of Robust and Nonlinear Control*, vol. 28, no. 14, pp. 4188–4208, 2018.
[23] C. Huang, X. Zhang, and G. Zhang, "Decentralized event-triggered cooperative path-following control for multiple autonomous surface vessels under actuator failures," *Applied Ocean Research*, vol. 113, p. 102751, 2021.
[24] Y. Lu, X. Xu, L. Qiao, and W. Zhang, "Robust adaptive formation tracking of autonomous surface vehicles with guaranteed performance and actuator faults," *Ocean Engineering*, vol. 237, p. 109592, 2021.
[25] W. Yue, X. Guan, and L. Wang, "Robust nonlinear multiple unmanned surface vessels control against probabilistic faults and time-varying delay," *IEEE Access*, vol. 7, pp. 143 263–143 272, 2019.
[26] W. Zhou, Y. Wang, C. K. Ahn, J. Cheng, and C. Chen, "Adaptive fuzzy backstepping-based formation control of unmanned surface vehicles with unknown model nonlinearity and actuator saturation," *IEEE Transactions on Vehicular Technology*, vol. 69, no. 12, pp. 14 749–14 764, 2020.
[27] G. Zhu, Y. Ma, Z. Li, R. Malekian, and M. Sotelo, "Event-triggered adaptive neural fault-tolerant control of underactuated msvs with input saturation," *IEEE Transactions on Intelligent Transportation Systems*, vol. 23, no. 7, pp. 7045–7057, 2022.
[28] L.-Y. Hao, H. Zhang, G. Guo, and H. Li, "Quantized sliding mode control of unmanned marine vehicles: various thruster faults tolerated with a unified model," *IEEE Transactions on Systems, Man, and Cybernetics: Systems*, vol. 51, no. 3, pp. 2012–2026, 2021.
[29] Z. Fei, X. Wang, and Z. Wang, "Event-based fault detection for unmanned surface vehicles subject to denial-of-service attacks," *IEEE Transactions on Systems, Man, and Cybernetics: Systems*, vol. 52, no. 5, pp. 3326–3336, 2022.
[30] Y. Ma, Z. Nie, S. Hu, Z. Li, R. Malekian, and M. Sotelo, "Fault detection filter and controller co-design for unmanned surface vehicles under dos attacks," *IEEE Transactions on Intelligent Transportation Systems*, vol. 22, no. 3, pp. 1422–1434, 2021.
[31] D. Zhang, G. Feng, Y. Shi, and D. Srinivasan, "Physical safety and cyber security analysis of multi-agent systems: A survey of recent advances," *IEEE/CAA Journal of Automatica Sinica*, vol. 8, no. 2, pp. 319–333, 2021.
[32] Y. Li, H. Fang, and J. Chen, "Anomaly detection and identification for multiagent systems subjected to physical faults and cyberattacks," *IEEE Transactions on Industrial Electronics*, vol. 67, no. 11, pp. 9724–9733, 2020.
[33] C. Liu, B. Jiang, X. Wang, H. Yang, and S. Xie, "Distributed fault-tolerant consensus tracking of multi-agent systems under cyber-attacks," *IEEE/CAA Journal of Automatica Sinica*, vol. 9, no. 6, pp. 1037–1048, 2022.
[34] C. Deng and C. Wen, "Distributed resilient observer-based fault-tolerant control for heterogeneous multiagent systems under actuator faults and dos attacks," *IEEE Transactions on Control of Network Systems*, vol. 7, no. 3, pp. 1308–1318, 2020.
[35] Z. Zhang and J. Dong, "Fault-tolerant containment control for it2 fuzzy networked multiagent systems against denial-of-service attacks and actuator faults," *IEEE Transactions on Systems, Man, and Cybernetics: Systems*, vol. 52, no. 4, pp. 2213–2224, 2022.
[36] X.-G. Guo, P.-M. Liu, J.-L. Wang, and C. K. Ahn, "Event-triggered adaptive fault-tolerant pinning control for cluster consensus of heterogeneous nonlinear multi-agent systems under aperiodic dos attacks," *IEEE Transactions on Network Science and Engineering*, vol. 8, no. 2, pp. 1941–1956, 2021.
[37] Q. Song, F. Liu, J. Cao, and W. Yu, "Pinning-controllability analysis of complex networks: an m-matrix approach," *IEEE Transactions on Circuits and Systems I: Regular Papers*, vol. 59, no. 11, pp. 2692–2701, 2012.